

# Predicting the Response of Breast Cancer to Neoadjuvant Therapy Using a Mechanically Coupled Reaction–Diffusion Model

Jared A. Weis<sup>1,2,3</sup>, Michael I. Miga<sup>1,2,3,4,5</sup>, Lori R. Arlinghaus<sup>1</sup>, Xia Li<sup>1</sup>, Vandana Abramson<sup>5,6</sup>, A. Bapsi Chakravarthy<sup>5,7</sup>, Praveen Pendyala<sup>7</sup>, and Thomas E. Yankeelov<sup>1,2,3,5,8,9</sup>

## Abstract

Although there are considerable data on the use of mathematical modeling to describe tumor growth and response to therapy, previous approaches are often not of the form that can be easily applied to clinical data to generate testable predictions in individual patients. Thus, there is a clear need to develop and apply clinically relevant oncologic models that are amenable to available patient data and yet retain the most salient features of response prediction. In this study we show how a biomechanical model of tumor growth can be initialized and constrained by serial patient-specific magnetic resonance imaging data, obtained at two time points early in the course of therapy (before initiation and following one cycle of therapy), to predict the response for individual patients with breast cancer undergoing neoadjuvant therapy. Using our mechanics coupled modeling approach, we are

able to predict, after the first cycle of therapy, breast cancer patients that would eventually achieve a complete pathologic response and those who would not, with receiver operating characteristic area under the curve (AUC) of 0.87, sensitivity of 92%, and specificity of 84%. Our approach significantly outperformed the AUCs achieved by standard (i.e., not mechanically coupled) reaction–diffusion predictive modeling (0.75), simple analysis of the tumor cellularity estimated from imaging data (0.73), and the Response Evaluation Criteria in Solid Tumors (0.71). Thus, we show the potential for mathematical model prediction for use as a prognostic indicator of response to therapy. The work indicates the considerable promise of image-driven biophysical modeling for predictive frameworks within therapeutic applications. *Cancer Res*; 75(22); 4697–707. ©2015 AACR.

## Major Findings

Using a mathematical model based on basic tissue mechanical properties and constrained by patient-specific imaging data can provide predictions of outcome that outperform conventional RECIST-based approaches.

## Introduction

Neoadjuvant therapy is often administered to patients with locally advanced breast cancer in order to reduce the tumor burden prior to surgery (10). Patients exhibiting pathologic complete response (pCR; defined as no residual viable tumor on histologic analysis in breast or nodes at the completion of therapy) demonstrate significantly enhanced disease-free progression/survival; thus, this metric has emerged as the gold standard for evaluating response to neoadjuvant therapy (11, 12). With numerous neoadjuvant therapy regimens available, and many more treatments emerging, reliable prediction of patients that will go on to achieve pCR is highly significant. If accurate predictions that the regimen is not effective can be made early in a patient's treatment, the treatment could be changed to another, potentially more effective approach, thereby avoiding unnecessary treatment-related toxicities and providing a greater chance of achieving pCR (13).

Assessing early treatment response with the goal of predicting pCR remains a challenging clinical problem with no current uniform approach. Because of their quantitative and noninvasive nature, imaging-based biomarkers are attractive surrogate metrics for response assessment. Several imaging-based metrics have been investigated as biomarkers for predicting response in the neoadjuvant setting (14–22), with many efforts focusing on monitoring changes in morphologic characteristics. However, morphology-based characteristics are downstream from the underlying treatment-induced biologic response, and are, therefore, indicative only of late stage response. More recent efforts have focused on using functional parameters available from quantitative magnetic

<sup>1</sup>Institute of Imaging Science, Vanderbilt University, Nashville, Tennessee. <sup>2</sup>Department of Radiology and Radiological Sciences, Vanderbilt University, Nashville, Tennessee. <sup>3</sup>Department of Biomedical Engineering, Vanderbilt University, Nashville, Tennessee. <sup>4</sup>Department of Neurosurgery, Vanderbilt University, Nashville, Tennessee. <sup>5</sup>Vanderbilt-Ingram Cancer Center, Vanderbilt University, Nashville, Tennessee. <sup>6</sup>Department of Medicine, Division of Hematology/Oncology, Vanderbilt University, Nashville, Tennessee. <sup>7</sup>Department of Radiation Oncology, Vanderbilt University, Nashville, Tennessee. <sup>8</sup>Department of Physics, Vanderbilt University, Nashville, Tennessee. <sup>9</sup>Department of Cancer Biology, Vanderbilt University, Nashville, Tennessee.

**Note:** Supplementary data for this article are available at Cancer Research Online (<http://cancerres.aacrjournals.org/>).

**Corresponding Authors:** Jared A. Weis, Vanderbilt University, VU Station B, Nashville, TN 37235. Phone: 615-322-3521; Fax: 615-343-7919; E-mail: [jared.a.weis@vanderbilt.edu](mailto:jared.a.weis@vanderbilt.edu); and Thomas E. Yankeelov, [thomas.yankeelov@vanderbilt.edu](mailto:thomas.yankeelov@vanderbilt.edu)

**doi:** 10.1158/0008-5472.CAN-14-2945

©2015 American Association for Cancer Research.

### Quick Guide to Model Equations and Assumptions

Our modeling approach uses serial diffusion weighted magnetic resonance imaging (DW-MRI) data of tumor cellularity obtained before and after the first cycle of neoadjuvant therapy to generate spatial estimates of tumor cell proliferation/death in response to therapy. Because of the timing of data acquisition, the estimated spatial proliferation term is based on measured changes in cell density with treatment and therefore represents the net difference between cell growth and death. To separately estimate cell growth and death rates independently, additional data would be required. We assume a constant antitumor effect in time during therapy, and use our estimates of proliferation/death to run the model forward in time to predict the residual tumor burden at the conclusion of therapy. DW-MRI data sets are fit to Eq. A to return apparent diffusion coefficient (ADC) values on a voxel-by-voxel basis:

$$ADC = \frac{\sum_{i=x,y,z} \ln(S_0/S_i)/b_i}{3}, \quad (\text{A})$$

where  $i$  is the direction of diffusion weighting,  $b_i$  is the amount of diffusion weighting imparted to the sample,  $S_0$  denotes the signal intensity in the absence of diffusion gradients, and  $S_i$  is the signal intensity in the presence of the diffusion-sensitizing gradient. Using Eq. B, the ADC data for voxels satisfying the dynamic contrast enhanced magnetic resonance imaging (DCE-MRI) threshold criteria of 80% enhancement (1) were transformed to an estimate of tumor cell number,  $N(\bar{x}, t)$ :

$$N(\bar{x}, t) = \theta \left( \frac{ADC_w - ADC(\bar{x}, t)}{ADC_w - ADC_{\min}} \right), \quad (\text{B})$$

where  $\theta$  is the carrying capacity (i.e., the total number of tumor cells that fit within a voxel),  $ADC_w$  is the ADC of free water at 37°C ( $3 \times 10^{-3} \text{ mm}^2/\text{s}$ ),  $ADC(\bar{x}, t)$  is the ADC value at position  $(x,y)$  in image space, and  $ADC_{\min}$  is the minimum ADC value measured within the tumor for each patient, which corresponds to the voxel with the largest number of cells. The carrying capacity,  $\theta$ , was calculated as the ratio of the imaging voxel volume to the assumed tumor cell volume, assuming spherical tumor cells with packing density of 0.7405 (2) and a nominal tumor cell radius of 10  $\mu\text{m}$  (tumor cell volume of 4189  $\mu\text{m}^3$ ). Details of this approach are provided in refs. 3 and 4.

The set of coupled, partial differential equations governing the tumor growth model is shown in Eqs. C–E:

$$\frac{\partial N(\bar{x}, t)}{\partial t} = \nabla \cdot (D \nabla N(\bar{x}, t)) + k(\bar{x}) N(\bar{x}, t) \left( 1 - \frac{N(\bar{x}, t)}{\theta} \right), \quad (\text{C})$$

$$D = D_0 e^{-\gamma \sigma_{vm}(\bar{x}, t)}, \quad (\text{D})$$

$$\nabla \cdot G \nabla \bar{u} + \nabla \frac{G}{1 - 2\nu} (\nabla \cdot \bar{u}) - \lambda \nabla N(\bar{x}, t) = 0. \quad (\text{E})$$

Equation C models the spatiotemporal rate of change of tumor cell number as the sum of random cell diffusion and logistic growth. The apparent cell diffusion term,  $D$ , is linked to surrounding tissue mechanics via Eq. D, where  $\sigma_{vm}$  is the von Mises stress,  $\gamma$  is an empirically derived coupling constant, and  $D_0$  is the diffusion of tumor cells in the absence of external stress (5). Eq. E defines linear elastic, isotropic mechanical equilibrium subject to an external expansive force determined by changes in tumor cell number,  $N(\bar{x}, t)$ , and a coupling constant  $\lambda$ . This equation governs the response of the displacement vector,  $u$ , to tumor cell growth.  $G$  represents shear modulus, an intrinsic mechanical property of breast and tumor tissue.

In this model, a growing tumor imparts an external force on the surrounding tissue, which induces tissue deformation. This "mass effect" is the phenomenon by which a growing tumor displaces surrounding tissue. The overall deformation serves to increase the total mechanical distortion energy of the tissue, which depends on the local tissue mechanical properties of the immediately surrounding tissue (breast fibroglandular tissue is typically reported to be twice as stiff as adipose tissue; ref. 6). As tumors have been shown to be sensitive to their mechanical microenvironment, exhibiting reduced outward growth/expansion in areas of high stress (7, 8), accumulated distortion energy serves to inhibit tumor invasiveness in our model through a mechano-inhibitory reduction in the apparent tumor cell diffusion coefficient,  $D$ . More details of the model implementation are provided in ref. 9.

We acquire DW-MRI data at two time points, prior to initiating therapy and after one cycle of therapy, and use Eq. A to calculate ADC values. These serial ADC maps are then transformed to estimate the tumor cell density distribution at each time point using Eq. B. We then fit these data to a model of tumor growth/response, Eqs. C–E, to yield estimates of tumor cell proliferation/death and diffusion. The estimated parameters are then used in conjunction with the model to predict, by projecting the model forward in time, the residual tumor burden at the conclusion of neoadjuvant therapy.

Major assumptions in our modeling approach include a reduction in dimensionality to two-dimensional analysis of central-slice MR data, constant proliferation/diffusion values throughout neoadjuvant therapy following initial parameter estimation, and the nature of the mechano-inhibitory effect on tumor cell diffusivity. We return to these important assumptions in the Discussion.

resonance imaging (MRI) techniques. For example, in the recent multisite American College of Radiology Imaging Network (ACRIN) 6657/Investigation of Serial Studies to Predict Your Therapeutic Response with Imaging And moLecular Analysis (I-SPY TRIAL) (22), Hylton and colleagues examined traditional clinical assessment combined with imaging morphologic measurements and contrast enhanced signal enhancement ratio (SER). A four-predictor multivariate statistical model (clinical size, longest diameter, volume, and SER) was shown to have receiver operator characteristic (ROC) area under the curve (AUC) of 0.73 for prediction of pCR at an early imaging time point, prior to the second cycle of neoadjuvant therapy. A preliminary extension of this approach to combine quantitative region of interest (ROI) and voxel-level analysis metrics from both dynamic contrast-enhanced (DCE) and diffusion-weighted (DW) MRI, efflux rate transfer constant ( $k_{ep}$ ), and apparent diffusion coefficient (ADC), respectively, in a multivariate regression statistical analysis showed promise for achieving a higher predictive ability, with AUC for pCR prediction of 0.87 at an early imaging time point, after the first cycle of neoadjuvant therapy (17). These studies extract a single parameter or sets of parameters from quantitative imaging data analysis and perform a statistical correlation to clinical outcomes. However, the physiologic interpretation of statistical combinations of extracted parameters as they pertain to pCR or reduction in tumor burden is often largely unknown.

One promising way to maximize the impact of quantitative noninvasive imaging data is to use mathematical models of tumor growth driven by early time point imaging data in order to determine and predict therapeutic response. Major advances in mathematical modeling of tumor growth have occurred, where sophisticated simulations can be generated that recapitulate many cellular and bulk-level aspects of tumor growth and treatment response (23–25). Unfortunately, many such models are fundamentally limited in that they cannot readily incorporate clinical data and require knowledge of many different parameters of tumor growth/status that are either impractical or impossible to measure clinically (e.g., immune response, extracellular matrix status, genetic mutations, etc.). As complex, multiparametric models often require an extensive array of model parameters either obtained from literature values or empirically derived, they cannot be practically applied to individual patients. Thus, the field of mathematical oncology has been limited to more fundamental investigations and patient-specific predictive modeling has only seen limited clinical application. There is a clear need to develop clinically relevant oncological models that are amenable to available patient data and yet retain the most salient features of response prediction (13).

We and others (4, 26–31) have recently suggested using quantitative *in vivo* imaging data to drive mathematical models of tumor growth for predicting response. Following parameterization, these models can then be projected forward in space and time to predict eventual tumor distribution outcomes on a patient-specific basis. Rather than taking a classical reductionist approach where each appropriate physiologic constituent tumor-associated process is described mathematically and coupled into a comprehensive, yet increasingly complex representation, we have chosen to begin with a more traditional spatiotemporal growth model that captures first-order effects. In this approach, we use patient-specific quantitative imaging data in two ways: (i) to fit the model-associated parameters and (ii) to guide decisions whether to add complexity to the model based not purely on the existence of more sophisticated

tumor-dynamic processes but rather how well incorporation can match patient outcome as determined at the time of surgery. We posit that systematically incorporating (additional) appropriate complexity to maximize clinical prediction, rather than constructing from the myriad of reduced fundamental interactions, has considerable merit for the ultimate realization of practical mathematical oncology in the clinical setting.

Recently, we have developed and shown preliminary results for a biomechanical modeling framework where tumor response is parameterized using data from both before and after the first cycle of neoadjuvant therapy and the model is driven forward in time to predict tumor burden at the time of surgery (9). The model is based on the standard reaction–diffusion equation of tumor growth/response, with terms to describe tumor cell diffusion and proliferation; in our formulation, the model is initialized and constrained using the serial imaging data. We extend this basic macroscopic tumor model to incorporate a mechano-inhibitory effect of surrounding tissue stroma on tumor cell diffusivity/motility. In this study, we build upon the previous efforts and apply patient-specific predictive modeling, constrained by quantitative imaging data, to a group of patients exhibiting a varying degree of response to therapy. We adopt a patient-scale spatio-temporal tumor growth model framework and allow readily available clinical imaging data to guide the determination of model parameters in a best-fit sense. The goal of this study is to determine if a patient-specific mechanically coupled reaction–diffusion model of tumor response to therapy can be used as a predictive indicator of pCR.

## Materials and Methods

### Subject description

An existing database of patients with breast cancer receiving quantitative MRI before ( $t_1$ ), after one cycle ( $t_2$ ), and at the conclusion ( $t_3$ ) of neoadjuvant therapy from a previous study (17) was utilized for this retrospective analysis. Briefly, 33 patients with stage II/III breast cancer who underwent neoadjuvant therapy as a component of their clinical care were selected for this study. Inclusion criteria were as follows: no prior systemic therapies for breast cancer and histologically documented invasive carcinoma of the breast with a sufficient risk of recurrence, based on pretreatment clinical parameters of size, grade, age, and nodal status, to warrant the use of neoadjuvant therapy. Neoadjuvant therapy was administered at the discretion of the treating medical oncologist based on pretreatment clinical parameters.

Tumor type was classified based on expression status for estrogen receptor (ER), progesterone receptor (PR), and human epidermal growth factor 2 (HER2) and categorized as ER and/or PR positive, HER2 positive, or triple-negative (ER, PR, and HER2 negative); see Table 1. Most patients with HER2 positive tumors received paclitaxel, carboplatin, and trastuzumab every 3 weeks for six cycles. Most patients with ER and/or PR positive tumors received doxorubicin and cyclophosphamide every 2 weeks for four cycles followed by 12 weekly cycles of paclitaxel. Most patients with triple-negative tumors participated in an ongoing clinical trial and received weekly cisplatin and paclitaxel with or without everolimus for 12 weeks. Response status was determined at the time of surgery by a pathologist as either pCR, which is defined as no residual viable tumor on histologic analysis of the breast or nodes at the completion of neoadjuvant therapy, or non-pCR, which designates any residual invasive tumor on histologic analysis in breast or

Weis et al.

**Table 1.** Patient and tumor characteristics of the study population

Patient no.	Age (years)	Tumor type	Tumor grade	Pathologic response	Days between $t_1$ and $t_2$	Therapeutic regimen
1	50	ER <sup>+</sup> and/or PR <sup>+</sup>	3	Non-pCR	14	AC→Taxol
2	52	HER2 <sup>+</sup>	3	Non-pCR	18	Taxotere
3	60	HER2 <sup>+</sup>	1	Non-pCR	13	AC→Taxol + concurrent trastuzumab
4	36	Triple negative	2	Non-pCR	7	Taxol + cisplatin ± everolimus
5	48	ER <sup>+</sup> and/or PR <sup>+</sup>	1	Non-pCR	14	Dose-dense AC→Taxol
6	43	ER <sup>+</sup> and/or PR <sup>+</sup>	2	Non-pCR	14	Dose-dense AC→Taxol
7	59	ER <sup>+</sup> and/or PR <sup>+</sup>	2	Non-pCR	28	Dose-dense AC→Taxol
8	53	Triple negative	2	Non-pCR	9	Taxol + cisplatin ± everolimus
9	35	HER2 <sup>+</sup>	3	Non-pCR	25	Trastuzumab + carboplatin + ixabepilone
10	28	Triple negative	3	Non-pCR	9	Taxol + cisplatin ± everolimus
11	33	ER <sup>+</sup> and/or PR <sup>+</sup>	3	Non-pCR	9	AC→Taxol
12	39	ER <sup>+</sup> and/or PR <sup>+</sup>	1	Non-pCR	13	AC→Taxol
13	57	Triple negative	3	Non-pCR	13	AC→Taxol
14	67	HER2 <sup>+</sup>	3	Non-pCR	11	Dose-dense AC→Taxol
15	45	Triple negative	3	Non-pCR	17	Taxol + cisplatin ± everolimus
16	46	HER2 <sup>+</sup>	3	Non-pCR	19	Taxotere + carboplatin + Herceptin
17	47	ER <sup>+</sup> and/or PR <sup>+</sup>	1	Non-pCR	17	Taxotere→AC
18	36	HER2 <sup>+</sup>	2	Non-pCR	15	AC→Taxol
19	43	HER2 <sup>+</sup>	3	Non-pCR	7	Cisplatin + Taxol ± everolimus
20	55	ER <sup>+</sup> and/or PR <sup>+</sup>	2	Non-pCR	24	AC→Taxol
21	58	ER <sup>+</sup> and/or PR <sup>+</sup>	2	Non-pCR	7	Cisplatin + Taxol ± everolimus
22	53	HER2 <sup>+</sup>	3	pCR	21	AC→concurrent Taxol + trastuzumab
23	46	ER <sup>+</sup> and/or PR <sup>+</sup>	3	pCR	13	Taxotere→AC
24	46	HER2 <sup>+</sup>	2	pCR	24	AC→concurrent Taxol + trastuzumab
25	33	Triple negative	3	pCR	15	AC→weekly Taxol
26	39	HER2 <sup>+</sup>	2	pCR	14	Trastuzumab + Lapatinib
27	46	ER <sup>+</sup> and/or PR <sup>+</sup>	3	pCR	13	AC→Taxol
28	42	Triple negative	3	pCR	15	Taxol + cisplatin ± everolimus
29	34	Triple negative	3	pCR	16	Taxotere→AC
30	44	HER2 <sup>+</sup>	3	pCR	7	Trastuzumab + Lapatinib
31	37	Triple negative	3	pCR	7	Taxol + cisplatin ± everolimus
32	39	Triple negative	3	pCR	14	AC→Taxol
33	48	HER2 <sup>+</sup>	3	pCR	29	Taxotere + carboplatin + Herceptin

nodes at the completion of neoadjuvant therapy. Participating patients provided informed written consent to an Institutional Review Board approved study. For more information on the patient population, the reader is referred to Li and colleagues (17).

#### Data acquisition

MRI was performed using a Philips 3T Achieva MR scanner (Philips Healthcare). A four-channel receive double-breast coil was used for 20 patients (Invivo), and a 16-channel double-breast coil was used for 13 patients. THRIVE ( $T_1$  high-resolution isotropic volume examination) anatomical data were acquired via a  $400 \times 400 \times 129$  acquisition matrix over a  $20 \text{ cm} \times 20 \text{ cm} \times 12.9 \text{ cm}$  transverse field of view (FOV) with one signal acquisition, and  $\text{TR}/\text{TE}/\alpha = 6.43 \text{ ms}/3.4 \text{ ms}/10^\circ$ . Dynamic contrast enhanced MRI (DCE-MRI) utilized an acquisition matrix of  $192 \times 192 \times 20$  (full breast) over a sagittal square FOV ( $22 \text{ cm} \times 22 \text{ cm}$ ) with slice thickness of 5 mm, one signal acquisition, and a SENSE factor of 2. Dynamic scans used a flip angle of  $20^\circ$ . Each dynamic set was collected in 16 s at 25 time points. A catheter placed within an antecubital vein delivered 0.1 mmol/kg (9–15 mL, depending on patient weight) of gadopentetate dimeglumine, Gd-DTPA (Magnevist) at 2 mL/s, followed by a saline flush, via a power injector (Medrad) after the acquisition of three baseline dynamic scans. DW-MRI was acquired with a single-shot spin echo (SE) echo planar imaging sequence in three orthogonal diffusion encoding directions, with  $b$ -values of 0 and 500 or 600  $\text{s}/\text{mm}^2$ , FOV of  $19.2 \text{ cm} \times 19.2 \text{ cm}$ , and an acquisition matrix of  $96 \times 96$  reconstructed to  $144 \times 144$ . SENSE parallel imaging (acceleration factor = 2)

and spectrally selective adiabatic inversion recovery fat saturation were implemented to reduce image artifacts. Subjects were breathing freely with no gating applied. The DW-MRIs consisted of 12 sagittal slices with slice thickness of 5 mm (no slice gap),  $\text{TR} = 3080 \text{ ms}$ ,  $\text{TE} = \text{"shortest"}$  (41 or 60 ms),  $\Delta = 19.8$  or 29 ms, and  $\delta = 10.7$  or 21 ms,  $\text{NSA} = 10$ . The total scan time for THRIVE, DCE-MRI, and DW-MRI data was approximately 2.7, 6.7, and 4.7 minutes, respectively.

#### Data analysis

A mechanically coupled reaction diffusion model of tumor response to therapy that used the MRI data obtained at time points  $t_1$  and  $t_2$  was used to predict tumor burden at the conclusion of neoadjuvant therapy. Although a brief description follows, the interested reader is referred to Weis and colleagues for details of the modeling methodology (9). Briefly, THRIVE, DCE-MRI, and DW-MRI data were longitudinally coregistered (32) across all time points. Central-slice images through the midpoint of the tumor were extracted from MRI volumes for further analysis. DCE-MRI data were used to define a tumor region-of-interest for voxels satisfying 80% signal enhancement threshold (9) between the precontrast images (i.e., the average signal intensity from DCE-MRI time points 1–3) and the postcontrast images (i.e., the average signal intensity from DCE-MRI time points 4–25). Voxels that showed a signal intensity increase more than the 80% threshold between the pre- and postcontrast data were defined as tumor (1). ADC maps were calculated from DW-MRI datasets using Eq. A

and transformed to estimates of tumor cell number using Eq. B (3, 4). A two-dimensional, mechanically coupled reaction diffusion tumor model, Eqs. C–E, was used to describe tumor cell logistic growth/decay and diffusion based on the central slice of the MR data. This model incorporates a tumor growth "mass effect" where accumulated mechanical distortion energy has an inhibitory effect on tumor cell invasiveness (5). Tumor cellularity at baseline ( $t_1$ ) and after one cycle of neoadjuvant therapy ( $t_2$ ) was used to estimate the spatially varying proliferation rates and a global tumor cell diffusion parameter by a conjugate-gradient nonlinear optimization. Following parameter fitting, the model was projected forward in time (using the estimated proliferation and tumor cell diffusion parameters) to the final time point at the conclusion of neoadjuvant therapy ( $t_3$ ), and the tumor cellularity was calculated as a model prediction. A schematic of the model parameter estimation and prediction framework is shown in Fig. 1. In addition, the cellularity maps for each patient at each time point for both the experimentally observed ( $t_1$  and  $t_2$ ) and model predicted ( $t_3$ ) cellularity data were summed to yield an estimate of the total tumor cellularity. To eliminate volumetric bias, these numbers are expressed as a percent change relative to a reference time point; for example, a percent change in cellularity from  $t_1$  to  $t_2$  is defined as  $100(t_2 - t_1)/t_1$ .

### Statistical analysis

Statistical analysis between non-pCR and pCR patient groups for percent changes in each analysis metric was performed using the Wilcoxon test. Statistical significance was set at  $P < 0.05$ .

Receiver operating characteristic (ROC) curves were generated for prediction of pCR for both the mechanically coupled model and a standard reaction–diffusion model. ROC curves were analyzed and area under the curve (AUC) and 95% confidence intervals (CI) were generated for each model. The optimal cutoff was selected utilizing the Youden index, which maximizes the difference between the true positive rate and the false positive rate (33). Data were analyzed using GraphPad Prism (GraphPad Software).

## Results

### Clinical patient data

Thirty-three patients (median age, 46; range, 28–67) completed scanning at  $t_1$  and at  $t_2$ . The median time between  $t_1$  and  $t_2$  was 14 days (range, 7–29 days). Table 1 summarizes the salient features of the patient data set, including their tumor type and pathologic response. After neoadjuvant therapy, 12 of 33 patients (36%) were defined as having achieved pCR.

### Representative imaging and modeling data

Imaging data and model predictions for tumors from two representative patients are shown in Figs. 2 and 3. Fig. 2 displays data from a patient that achieved pCR at the conclusion of neoadjuvant therapy that was scanned before, after the first cycle, and at the conclusion of neoadjuvant therapy in the form of anatomical images (Fig. 2A–C), ADC (from DW-MRI) values superimposed on the averaged postcontrast images (Fig. 2D–F), and the estimated cellularity (using Eq. B) as a fraction of the carrying capacity (Fig. 2G–I). The mechanically coupled reaction–diffusion model is used to reconstruct parameter estimates of global diffusion and spatial proliferation rate (Fig. 2J) based on observed cellularity data from the baseline and post-one cycle

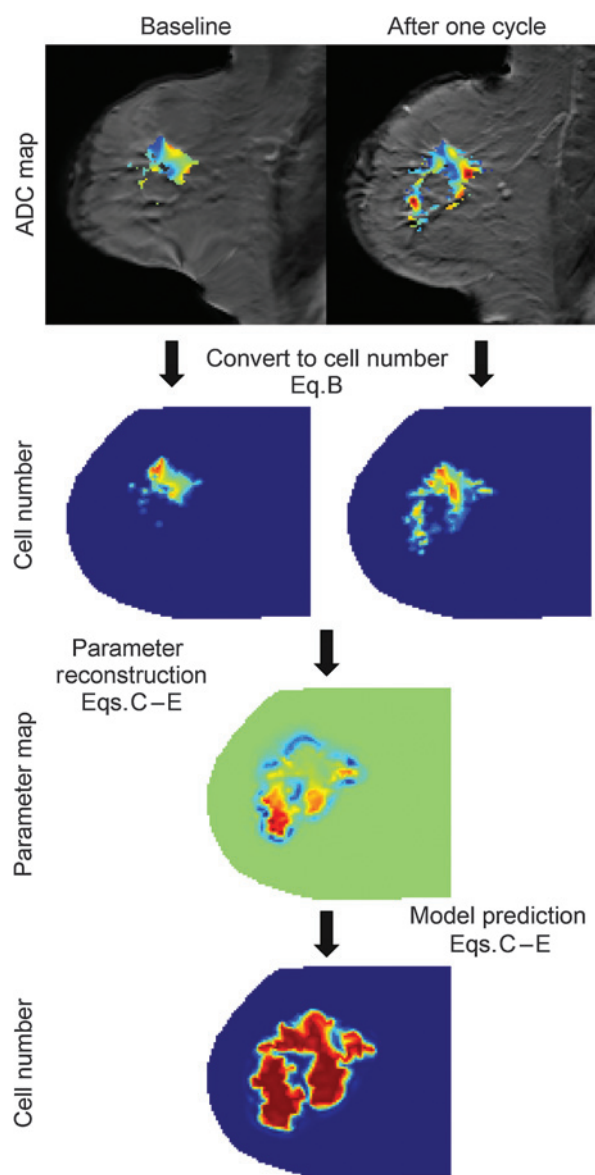
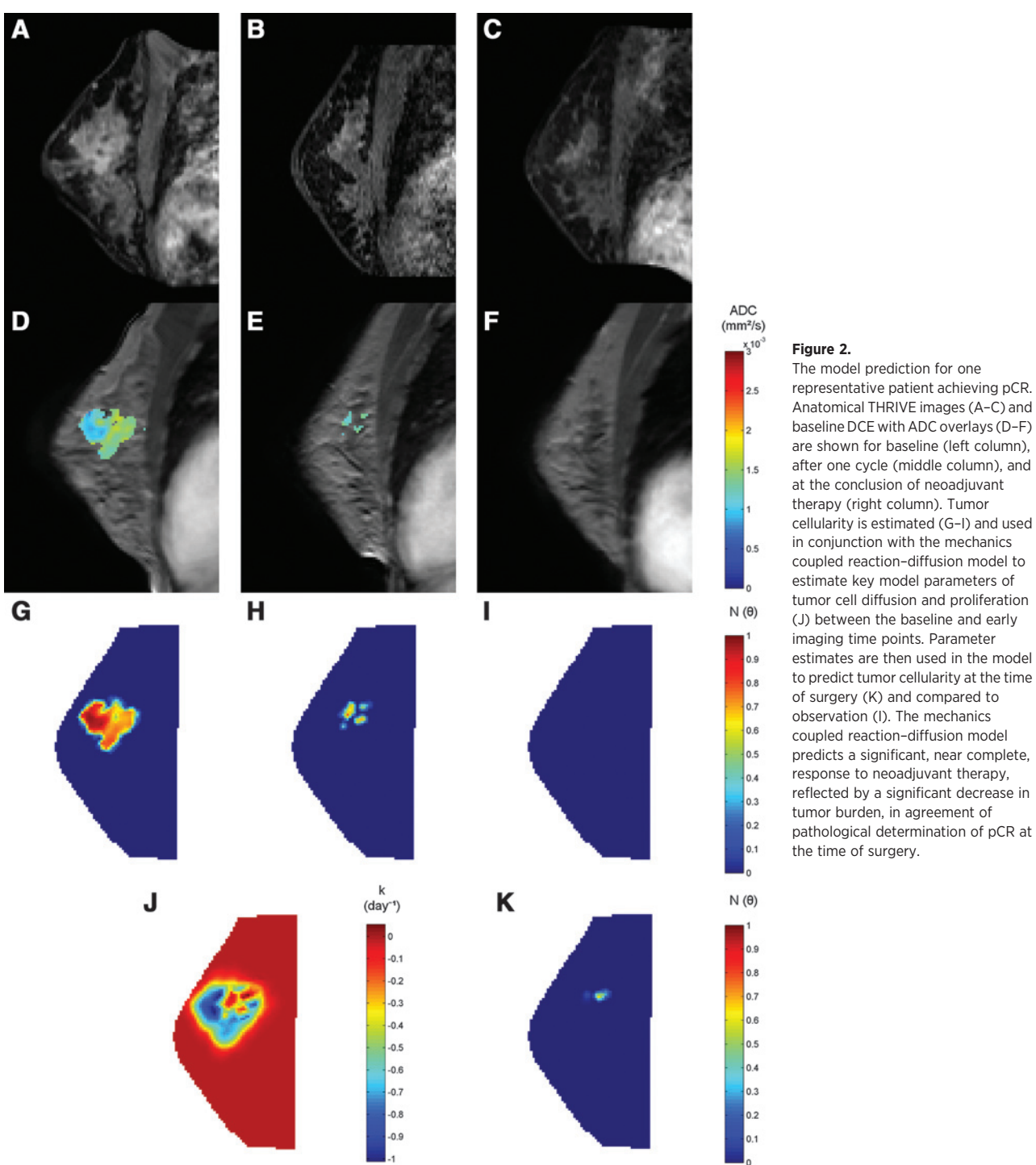


**Figure 1.**

Schema of patient-specific mathematical modeling response prediction framework. ADC maps at baseline and after one cycle of neoadjuvant therapy are converted to tumor cellularity. The mathematical model is then used to reconstruct parameter estimates of cellular proliferation and diffusion between these two time points. The model is then evaluated forward in time to predict the pathologic response at the time of surgery.

time points. The model is then evaluated forward in time based on the estimated parameters and observed cellularity data in order to predict cellularity at the conclusion of neoadjuvant therapy (Fig. 2K). Model prediction strongly agrees with data observations from imaging and pathology of complete response to therapy. Qualitatively, the estimated cellularity map is shown to exhibit a significant trend of decrease between  $t_1$  and  $t_2$ . The prediction of the mechanically coupled reaction–diffusion model is seen to continue the trend of decreasing cellularity at  $t_3$ , with a prediction of near complete response. Figure 3 displays similar data for a representative patient with residual disease at the time of surgery

Weis et al.



(i.e., a non-pCR). The estimated cellularity map for this patient exhibits an opposite trend from that of the pCR patient, with increasing estimated cellularity observations from  $t_1$  to  $t_2$ . The mechanically coupled reaction-diffusion model prediction is then shown to predict a lack of response to therapy with an increase in cellularity at  $t_3$ . Compared to observed cellularity data, the model overpredicts cellularity at the final time point. Combined, representative images and associated estimated parameter

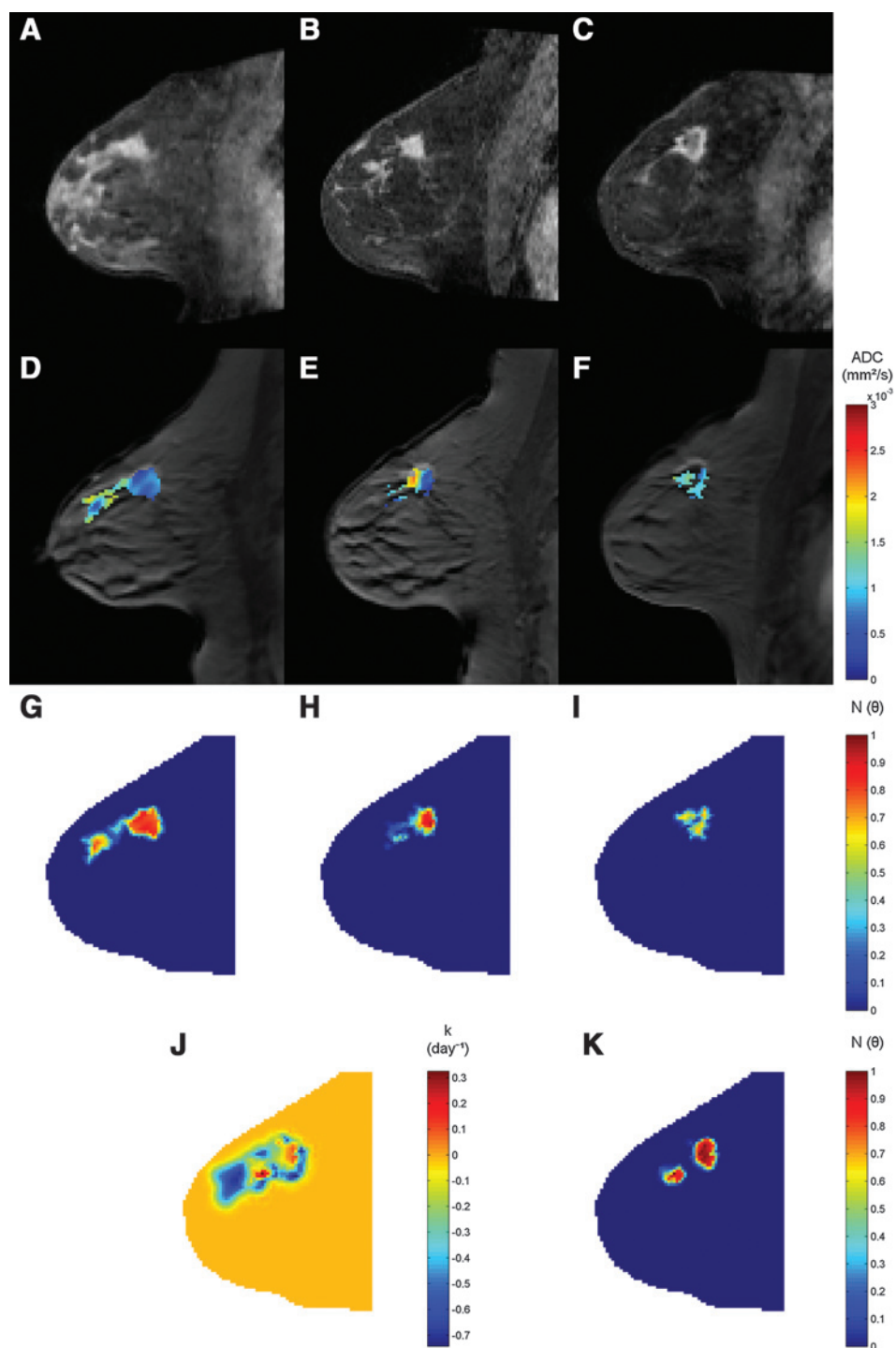
maps of proliferation rates depict overall prediction of regression of disease for a responding patient and significant progression of disease for a nonresponding patient.

#### Predictive performance of analysis metrics

Table 2 reports the overall performance for predicting pCR from a group of 33 patients exhibiting a varying degree of responsiveness to neoadjuvant therapy for analysis metrics based on RECIST

**Figure 3.**

The model prediction for one representative patient not achieving pCR. Anatomical THRIVE images (A–C) and baseline DCE with ADC overlays (D–F) are shown for baseline (left column), after one cycle (middle column), and at the conclusion of neoadjuvant therapy (right column). Tumor cellularity is estimated (G–I) and used in conjunction with the mechanics coupled reaction–diffusion model to estimate key model parameters of tumor cell diffusion and proliferation (J) between the baseline and early imaging time points. Parameter estimates are then used in the model to predict tumor cellularity at the time of surgery (K) and compared to observation (I). The mechanics coupled reaction–diffusion model predicts a lack of response to neoadjuvant therapy, reflected by a significant increase in tumor burden, in agreement of pathologic determination of non-pCR at the time of surgery.



(i.e., measurement of tumor longest dimension), observed cellularity (based on ADC values from DW-MRI), reaction–diffusion model prediction, and mechanics coupled reaction–diffusion model prediction. Area under the receiver operating characteristic curve, sensitivity, and specificity are reported for each metric, along with 95% confidence intervals. Figure 4 depicts the average value, 95% confidence interval as indicated by error bars, and  $P$

value for comparisons between non-pCR and pCR tumors for each analysis metric, along with ROC curves.

Simple analysis of differences in tumor morphologic and cellularity observations before and after the first cycle of neoadjuvant therapy exhibit a modest ability to predict pCR status at the conclusion of therapy. The change in tumor longest dimension between imaging time points  $t_1$  and  $t_2$ , based on RECIST criteria,

Weis et al.

**Table 2.** Table of ROC analysis parameters for RECIST, cellularity (input data to model), reaction–diffusion model, and mechanics coupled model

Analysis metric	AUC (95% CI)	Sensitivity % (95% CI)	Specificity % (95% CI)
RECIST % change $t_1$ to $t_2$	0.71 (0.53–0.90)	92 (62–100)	53 (29–76)
Cellularity % change $t_1$ to $t_2$	0.73 (0.55–0.91)	100 (74–100)	47 (24–71)
Reaction diffusion model % change $t_2$ to $t_3$	0.75 (0.58–0.92)	100 (75–100)	55 (32–77)
Mechanics coupled model % change $t_2$ to $t_3$	0.87 (0.74–1.0)	92 (62–100)	84 (60–97)

NOTE: % change  $t_1$  to  $t_2'$  denotes observed cellularity or RECIST measures at the post one cycle time point expressed as a percent change to the initial time point. Similarly, % change  $t_2$  to  $t_3'$  denotes model predicted cellularity at the final time point expressed as a percent change to the post one cycle time point.

reflect an AUC and sensitivity of 0.71% and 92%, respectively; however, RECIST exhibits a poor specificity of 53% in this study. Similarly, the estimated tumor cellularity based on ADC values from DW-MRI is shown to have modest predictive performance, with ROC AUC and sensitivity of 0.73% and 100%, respectively, and poor specificity of 47%.

Using image-based mathematical modeling in order to predict tumor response to therapy is seen to improve pCR predictive performance. Reaction–diffusion model predictions of tumor cellularity at the conclusion of neoadjuvant therapy, expressed as a percent change from cellularity after one cycle of neoadjuvant therapy, exhibit an AUC, sensitivity, and specificity of 0.75%, 100%, and 55%, respectively. Here, model predictions are expressed as a percent change to eliminate volumetric bias from prediction results. Incorporating mechanical coupling into the reaction–diffusion model significantly improves pCR predictive performance, achieving an ROC AUC, sensitivity, and specificity of 0.87%, 92%, and 84%, respectively.

## Discussion

We previously introduced a novel mathematical framework for predictive modeling that is centered on integrating quantitative *in vivo* imaging data with biomechanical models of tumor growth (9). This approach represents a significant departure from existing paradigms in mathematical oncology modeling by using patient-specific data to parameterize a model that can then be used to make a prediction at a future time point that can then be checked directly against patient response. In this work, we retrospectively apply this framework to a database of patients exhibiting varying degrees of responsiveness to neoadjuvant therapy. We compared model predictions of responsiveness to pathologic response assessment at the time of surgery. Our results demonstrate a significant predictive ability of our mechanics coupled modeling approach in identifying patients that would go on to achieve pCR, as indicated by a strong AUC of 0.87. Our mechanics coupled reaction–diffusion modeling approach significantly outperformed other, commonly used metrics, including analysis of tumor longest dimension (i.e., RECIST), early-cycle changes in DW-MRI (used as empirical input data to the models), and standard reaction–diffusion predictive modeling. Compared with the standard reaction–diffusion model, the mechanically coupled model exhibits significantly improved prediction specificity, reflected by improved prediction of true non-pCR patients (55% vs. 84%, respectively). Further analysis of the patients for which mechanically coupled modeling improved predictability over standard modeling (data not shown), failed to reveal correlations with any other known factor (including breast density, patient age, and breast cancer subtype, among others).

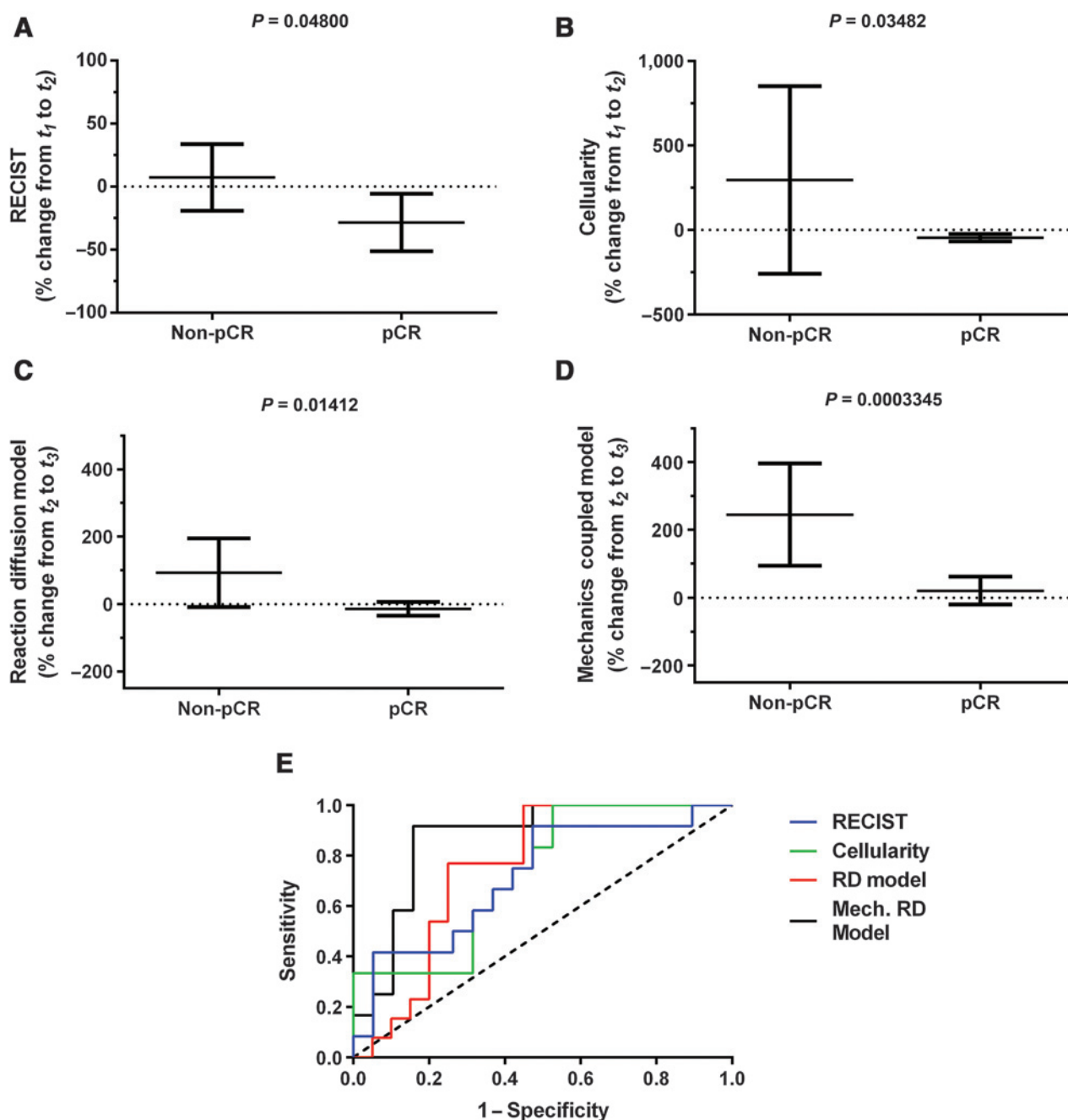
Our results also confirm previous reports of the use of early cycle DW-MRI ADC data alone in predicting neoadjuvant therapy response (34–39). Trends of decreasing/increasing cellularity are

clearly visible between the observed cellularity before and after the first cycle of therapy, as shown in Figs. 2 and 3, with predictive AUC of 0.73. However, analysis of these data is seen to exhibit limited specificity, as has been previously demonstrated (35, 40).

The results from this study are promising, but we recognize that there are several limitations in our current approach. First, we estimate the key model parameters (i.e., proliferation and tumor cell diffusion) from data obtained before and after the first cycle of neoadjuvant therapy; this is an admittedly (temporally) sparse set of measurements for attempting to capture the dynamics through a model fitting procedure. In addition, we have assumed that reconstructed model parameters do not vary in time; this is essentially equivalent to assuming a constant antitumor effect during neoadjuvant therapy treatment and this is clearly a simplification of the response of tumor cells to neoadjuvant therapy. True response undoubtedly exhibits strong nonlinear temporal response to therapy; indeed, the evolution of a resistant phenotype in the presence of continued chemotherapeutic administration speaks directly to a nonlinear effect that is not currently taken into account in our approach. However, it is clinically infeasible to acquire sufficient imaging time points throughout the course of therapy to accurately predict the temporal changes in proliferation rates and tumor cell diffusion with the current model. We are currently exploring acquisition of one additional early imaging time point, collected after two cycles of therapy, in order to better understand the temporal evolution of parameters and more accurate prediction of response.

A second limitation, as also noted in Li and colleagues (17), is the variation in the breast cancer subtype, therapeutic regimen (including the specific therapeutic agent and dosing frequency), and number of days elapsed between imaging time points,  $t_1$  and  $t_2$ . Thus, it is possible that the modeling approach could be influenced by the underlying dynamics and biology of specific breast cancer subtypes as well as the particular therapy regimen utilized. This source of uncertainty due to patient-specific biologic variability is particularly difficult to control, due to the nature of clinical research data acquisition constraints. It will be important, as a greater number of patients are analyzed with this methodology, to statistically analyze the model relative to cancer subtype, therapeutic regimen, and imaging time point delay to determine these effects. In addition, future work toward model validation in preclinical and *in vitro* systems will facilitate greater experimental control and provide further understanding toward model robustness in the presence of such biological variability. Of course, the encouraging preliminary results achieved with our modeling approach in spite of this variability points to the importance, and potential generalizability, of using models based on patient-specific information.

Another limitation is that our current approach utilizes central-slice MR data to initialize and constrain two-dimensional mathematical models, rather than using full image volumes and three-dimensional models. We do note, however, that we are utilizing

**Figure 4.**

Tumors from patients either achieving pCR or not were assessed as a percent change from  $t_1$  to  $t_2$  by RECIST criteria (A) and observed cellularity (B) and as a percent change from  $t_2$  to predicted  $t_3$  by reaction diffusion model prediction (C) and mechanics coupled model prediction (D). Data are expressed as mean with 95% confidence intervals, with  $P$  values indicated for statistically significant differences between groups. ROC curves for all analysis metrics are shown along with the dashed line of identity (E).

somewhat thick slices, 5 mm, due to the spatio-temporal acquisition requirements of the trial for which the MRI data were originally acquired. Extension of our approach to three-dimensional analysis is straightforward, and we would expect an enhanced predictive capability through the use of additional volumetric data. However, the current computational demands for iterative reconstruction of volumetric parameter maps

significantly limit the feasibility of extending our approach to three-dimensional analysis for an entire patient database at this time. Currently, efforts are underway to refine our approach by exploring significant computational speed enhancements through the use of high-performance computing cluster and/or graphics processing unit processing in addition to algorithmic enhancements.

Weis et al.

The mechanically coupled reaction diffusion model adds two additional degrees of freedom to each node in the finite element mesh (in addition to the existing degree of freedom for tumor cell number) due to the need for calculation of a displacement solution. This added complexity increases the computation time for the forward model by approximately 40%, without parallelization of matrix assembly and/or matrix inversion. In addition, the impact on total wall-clock time is relatively limited as the entire mechanically coupled reaction diffusion model prediction approach typically requires only 1 to 2 hours for each patient.

At present, our mechanics coupled approach relies on the use of literature values for the elastic properties of the breast (9). In addition, our approach currently ignores other important biologic factors beyond simple growth and mechano-inhibitory diffusion. Other ongoing efforts are designed to address these limitations through incorporation of additional quantitative patient-specific imaging methodologies to inform more complex models (13).

Given these limitations, we note that our approach compares very favorably, with similar AUC, to previous multimodal statistical regression analysis of this same patient population in previous work that combines ROI and voxel-level DW-MRI and DCE-MRI analysis (17). Importantly, our approach currently includes data from only one quantitative imaging source, DW-MRI. Contrast-enhanced MRI data are used in this work only to identify tumor ROI, with no sensitivity to pharmacokinetic parameters fit from dynamic DCE-MRI data. It is therefore very encouraging that our model-based analysis framework, based on unimodal and two-dimensional central-slice input data, achieves similar predictive results to multimodal full-volume analysis.

In summary, we have demonstrated a model-based analysis method that provides predictions of therapeutic response using patient-specific early time point imaging data within the course of therapy. The framework provides good agreement with pathologic response observations as demonstrated by a strong predictive ability. The results suggest that an imaging-driven biophysically constrained modeling approach that combines reaction-diffusion with mechanical effects is a predictive indicator of response to therapy. Future work will seek to further enhance the predictive capacity of our approach by expanding the math-

ematical model of tumor response to include model terms that can be populated with other sources of quantitative patient-specific noninvasive imaging, including DCE-MRI, fludeoxyglucose positron emission tomography (FDG-PET), and magnetic resonance elastography (MRE).

### Disclosure of Potential Conflicts of Interest

No potential conflicts of interest were disclosed.

### Authors' Contributions

**Conception and design:** J.A. Weis, M.I. Miga, T.E. Yankeelov  
**Development of methodology:** J.A. Weis, M.I. Miga, T.E. Yankeelov  
**Acquisition of data (provided animals, acquired and managed patients, provided facilities, etc.):** J.A. Weis, L.R. Arlinghaus, V. Abramson, A.B. Chakravarthy, T.E. Yankeelov  
**Analysis and interpretation of data (e.g., statistical analysis, biostatistics, computational analysis):** J.A. Weis, X. Li, T.E. Yankeelov  
**Writing, review, and/or revision of the manuscript:** J.A. Weis, M.I. Miga, L.R. Arlinghaus, X. Li, V. Abramson, A.B. Chakravarthy, T.E. Yankeelov  
**Administrative, technical, or material support (i.e., reporting or organizing data, constructing databases):** J.A. Weis, A.B. Chakravarthy, P. Pendyala  
**Study supervision:** J.A. Weis, A.B. Chakravarthy, T.E. Yankeelov

### Acknowledgments

The authors offer their sincerest appreciation to the women who volunteered to participate in this study. The authors thank the National Institutes of Health for funding through NCI 1U01CA142565, NCI U01CA174706, NCI R25CA092043, NCI 1P50 098131, NCI P30CA68485, NCI R01CA138599, and NINDS 2R01NS049251. The authors also thank the Kleberg Foundation for generous support of the imaging program at Vanderbilt and the support provided by the Vanderbilt Initiative in Surgery and Engineering Pilot Award Program.

### Grant Support

This work was supported by the National Institutes of Health: NCI 1U01CA142565, NCI U01CA174706, NCI R25CA092043, NCI 1P50 098131, NCI P30CA68485, NCI R01CA138599, and NINDS 2R01NS049251

The costs of publication of this article were defrayed in part by the payment of page charges. This article must therefore be hereby marked *advertisement* in accordance with 18 U.S.C. Section 1734 solely to indicate this fact.

Received October 3, 2014; revised May 26, 2015; accepted July 29, 2015; published OnlineFirst September 2, 2015.

### References

- Li X, Arlinghaus LR, Ayers GD, Chakravarthy AB, Abramson RG, Abramson VG, et al. DCE-MRI analysis methods for predicting the response of breast cancer to neoadjuvant chemotherapy: pilot study findings. *Magn Reson Med* 2014;71:1592-602.
- Martin I, Dozin B, Quarto R, Cancedda R, Beltrame F. Computer-based technique for cell aggregation analysis and cell aggregation in *in vitro* chondrogenesis. *Cytometry* 1997;28:141-6.
- Anderson AW, Xie J, Pizzonia J, Bronen RA, Spencer DD, Gore JC. Effects of cell volume fraction changes on apparent diffusion in human cells. *Magn Reson Imaging* 2000;18:689-95.
- Atuegwu NC, Colvin DC, Loveless ME, Xu L, Gore JC, Yankeelov TE. Incorporation of diffusion-weighted magnetic resonance imaging data into a simple mathematical model of tumor growth. *Phys Med Biol* 2012;57:225-40.
- Garg I, Miga MI. Preliminary investigation of the inhibitory effects of mechanical stress in tumor growth. *SPIE Medical Imaging 2008: Visualization, Image-Guided Procedures, and Modeling Conference* 2008;6918:69182L1-11.
- McKnight AL, Kugel JL, Rossman PJ, Manduca A, Hartmann LC, Ehman RL. MR elastography of breast cancer: Preliminary results. *Am J Roentgenol* 2002;178:1411-7.
- Helmlinger G, Netti PA, Lichtenbeld HC, Melder RJ, Jain RK. Solid stress inhibits the growth of multicellular tumor spheroids. *Nat Biotechnol* 1997;15:778-83.
- Levental KR, Yu H, Kass L, Lakins JN, Egeblad M, Erler JT, et al. Matrix crosslinking forces tumor progression by enhancing integrin signaling. *Cell* 2009;139:891-906.
- Weis JA, Miga MI, Arlinghaus LR, et al. A mechanically coupled reaction-diffusion model for predicting the response of breast tumors to neoadjuvant chemotherapy. *Phys Med Biol* 2013;58:5851-66.
- Kaufmann M, von Minckwitz G, Bear HD, Buzdar A, McGale P, Bonnefoi H, et al. Recommendations from an international expert panel on the use of neoadjuvant (primary) systemic treatment of operable breast cancer: new perspectives 2006. *Ann Oncol* 2007;18:1927-34.
- Chollet P, Amat S, Cure H, de Latour M, LeBouedec G, Mouret-Reynier MA, et al. Prognostic significance of a complete pathological response after induction chemotherapy in operable breast cancer. *Br J Cancer* 2002;86:1041-6.
- Wolff AC, Berry D, Carey LA, Colleoni M, Dowsett M, Ellis M, et al. Research issues affecting preoperative systemic therapy for operable breast cancer. *J Clin Oncol* 2008;26:806-13.

13. Yankeelov TE, Atuegwu N, Hormuth D, Weis JA, Barnes SL, Miga MI, et al. Clinically relevant modeling of tumor growth and treatment response. *Sci Transl Med* 2013;5:187ps9.
14. Abramson RG, Li X, Hoyt TL, Su PF, Arlinghaus LR, Wilson KJ, et al. Early assessment of breast cancer response to neoadjuvant chemotherapy by semi-quantitative analysis of high-temporal resolution DCE-MRI: preliminary results. *Magn Reson Imaging* 2013;31:1457–64.
15. Atuegwu NC, Li X, Arlinghaus LR, Abramson RG, Williams JM, Chakravarthy AB, et al. Longitudinal, intermodality registration of quantitative breast PET and MRI data acquired before and during neoadjuvant chemotherapy: preliminary results. *Med Phys* 2014;41:052302.
16. Huang W, Li X, Chen Y, Chang MC, Oborski MJ, Malyarenko DI, et al. Variations of dynamic contrast-enhanced magnetic resonance imaging in evaluation of breast cancer therapy response: a multicenter data analysis challenge. *Transl Oncol* 2014;7:153–66.
17. Li X, Kang H, Arlinghaus LR, Abramson RG, Chakravarthy AB, Abramson VG, et al. Analyzing Spatial Heterogeneity in DCE- and DW-MRI parametric maps to optimize prediction of pathologic response to neoadjuvant chemotherapy in breast cancer. *Transl Oncol* 2014;7:14–22.
18. Li J, Jamin Y, Boulton JK, Cummings C, Waterton JC, Ulloa J, et al. Tumour biomechanical response to the vascular disrupting agent ZD6126 in vivo assessed by magnetic resonance elastography. *Br J Cancer* 2014;110:1727–32.
19. Cho N, Im SA, Park IA, Lee KH, Li M, Han W, et al. Breast cancer: early prediction of response to neoadjuvant chemotherapy using parametric response maps for MR imaging. *Radiology* 2014;272:385–96.
20. Cheung YC, Chen SC, Su MY, See LC, Hsueh S, Chang HK, et al. Monitoring the size and response of locally advanced breast cancers to neoadjuvant chemotherapy (weekly paclitaxel and epirubicin) with serial enhanced MRI. *Breast Cancer Res Treat* 2003;78:51–8.
21. Abraham DC, Jones RC, Jones SE, Cheek JH, Peters GN, Knox SM, et al. Evaluation of neoadjuvant chemotherapeutic response of locally advanced breast cancer by magnetic resonance imaging. *Cancer* 1996;78:91–100.
22. Hylton NM, Blume JD, Bernreuter WK, Pisano ED, Rosen MA, Morris EA, et al. Locally advanced breast cancer: MR imaging for prediction of response to neoadjuvant chemotherapy—results from ACRIN 6657/I-SPY TRIAL. *Radiology* 2012;263:663–72.
23. Brocato T, Dogra P, Koay EJ, Day A, Chuang Y-L, Wang Z, et al. Understanding Drug Resistance in Breast Cancer with Mathematical Oncology. *Curr Breast Cancer Rep* 2014;6:110–20.
24. Wang Z, Butner JD, Kerketta R, Cristini V, Deisboeck TS. Simulating cancer growth with multiscale agent-based modeling. *Semin Cancer Biol* 2015;30:70–8.
25. Quaranta V, Tyson DR. What lies beneath: looking beyond tumor genetics shows the complexity of signaling networks underlying drug sensitivity. *Sci Signal* 2013;6:pe32.
26. Harpold HL, Alvord EC Jr., Swanson KR. The evolution of mathematical modeling of glioma proliferation and invasion. *J Neuropathol Exp Neurol* 2007;66:1–9.
27. Rockne R, Rockhill JK, Mrugala M, Spence AM, Kalet I, Hendrickson K, et al. Predicting the efficacy of radiotherapy in individual glioblastoma patients in vivo: a mathematical modeling approach. *Phys Med Biol* 2010;55:3271–85.
28. Swanson KR, Rockne RC, Claridge J, Chaplain MA, Alvord EC Jr., Anderson AR. Quantifying the role of angiogenesis in malignant progression of gliomas: in silico modeling integrates imaging and histology. *Cancer Res* 2011;71:7366–75.
29. Szeto MD, Chakraborty G, Hadley J, Rockne R, Muzi M, Alvord EC Jr., et al. Quantitative metrics of net proliferation and invasion link biological aggressiveness assessed by MRI with hypoxia assessed by FMISO-PET in newly diagnosed glioblastomas. *Cancer Res* 2009;69:4502–9.
30. Wang CH, Rockhill JK, Mrugala M, Peacock DL, Lai A, Jusenius K, et al. Prognostic significance of growth kinetics in newly diagnosed glioblastomas revealed by combining serial imaging with a novel biomathematical model. *Cancer Res* 2009;69:9133–40.
31. Baldock AL, Yagle K, Born DE, Ahn S, Trister AD, Neal M, et al. Invasion and proliferation kinetics in enhancing gliomas predict IDH1 mutation status. *Neuro Oncol* 2014;16:779–86.
32. Li X, Dawant BM, Welch EB, Chakravarthy AB, Freehardt D, Mayer I, et al. A nonrigid registration algorithm for longitudinal breast MR images and the analysis of breast tumor response. *Magn Reson Imaging* 2009;27:1258–70.
33. Perkins NJ, Schisterman EF. The inconsistency of "optimal" cutpoints obtained using two criteria based on the receiver operating characteristic curve. *Am J Epidemiol* 2006;163:670–5.
34. Pickles MD, Gibbs P, Lowry M, Turnbull LW. Diffusion changes precede size reduction in neoadjuvant treatment of breast cancer. *Magn Reson Imaging* 2006;24:843–7.
35. Sharma U, Danishad KK, Seenu V, Jagannathan NR. Longitudinal study of the assessment by MRI and diffusion-weighted imaging of tumor response in patients with locally advanced breast cancer undergoing neoadjuvant chemotherapy. *NMR Biomed* 2009;22:104–13.
36. Belli P, Costantini M, Ierardi C, et al. Diffusion-weighted imaging in evaluating the response to neoadjuvant breast cancer treatment. *Breast J* 2011;17:610–9.
37. Woodhams R, Kakita S, Hata H, Iwabuchi K, Kuranami M, Gautam S, et al. Identification of residual breast carcinoma following neoadjuvant chemotherapy: diffusion-weighted imaging—comparison with contrast-enhanced MR imaging and pathologic findings. *Radiology* 2010;254:357–66.
38. Nilsen L, Fangberget A, Geier O, Olsen DR, Seierstad T. Diffusion-weighted magnetic resonance imaging for pretreatment prediction and monitoring of treatment response of patients with locally advanced breast cancer undergoing neoadjuvant chemotherapy. *Acta Oncol* 2010;49:354–60.
39. Fujimoto H, Kazama T, Nagashima T, Sakakibara M, Suzuki TH, Okubo Y, et al. Diffusion-weighted imaging reflects pathological therapeutic response and relapse in breast cancer. *Breast Cancer* 2014;21:724–31.
40. Hahn SY, Ko EY, Han BK, Shin JH, Ko ES. Role of diffusion-weighted imaging as an adjunct to contrast-enhanced breast MRI in evaluating residual breast cancer following neoadjuvant chemotherapy. *Eur J Radiol* 2014;83:283–8.

# Cancer Research

The Journal of Cancer Research (1916–1930) | The American Journal of Cancer (1931–1940)

## Predicting the Response of Breast Cancer to Neoadjuvant Therapy Using a Mechanically Coupled Reaction–Diffusion Model

Jared A. Weis, Michael I. Miga, Lori R. Arlinghaus, et al.

*Cancer Res* 2015;75:4697-4707. Published OnlineFirst September 2, 2015.

**Updated version** Access the most recent version of this article at:  
doi:[10.1158/0008-5472.CAN-14-2945](https://doi.org/10.1158/0008-5472.CAN-14-2945)

**Cited articles** This article cites 38 articles, 10 of which you can access for free at:  
<http://cancerres.aacrjournals.org/content/75/22/4697.full.html#ref-list-1>

**E-mail alerts** [Sign up to receive free email-alerts](#) related to this article or journal.

**Reprints and Subscriptions** To order reprints of this article or to subscribe to the journal, contact the AACR Publications Department at [pubs@aacr.org](mailto:pubs@aacr.org).

**Permissions** To request permission to re-use all or part of this article, contact the AACR Publications Department at [permissions@aacr.org](mailto:permissions@aacr.org).